ACI MATERIALS JOURNAL TECHNICAL PAPER

Title No. 121-M19

Relation between Strength and Yield Stress in Fiber-Reinforced Mortar

by Ronan Chometon, Maxime Liard, Pascal Hébraud, and Didier Lootens

The need to constantly improve the quality and properties of manufactured products leads to the development of hybrid materials that combine different elements, complementing one another. Fiber-reinforced mortar is one of those products, as the fibers are used to improve cementitious materials' flexural weakness. Experimental data on different metallic fibers dispersed in mortar demonstrate the correlation between early-age rheological properties and long-term mechanical strength. Both quantities depend on the ratio of the solid volume fraction of the fiber to a critical solid volume fraction characteristic of the form factors of the fiber. It is demonstrated that both effects arise from the packing stress of the fibers in the mortar when their concentrations are close to their maximum packing fraction. Geometrical arguments are used to explain how this critical volume fraction is related to the fiber form factor. Then, it enables the building of master curves using geometrical arguments.

Keywords: critical volume fraction; fiber-reinforced mortar; flexural strength; master curves; mortar; rheology.

INTRODUCTION

The need to reduce the quantity of construction materials drives the industry to develop new materials with more diverse and advanced properties. Most construction materials should be kept affordable as the amount needed is significant and essentially obtained from cheap local raw materials. Most of the time, these materials fulfill one property—such as structural, acoustic, or thermal—and should be used in combination with several other materials glued together to build sandwich walls. Developing composite or hybrid materials whose properties are a combination of their constitutive components' properties could then be a solution to limit the number of layers required for the sandwich walls, reducing the number of materials and simplifying the recycling process. The main difficulty of a hybrid formulation is ensuring the positive interactions between its different elements: the aim is to collect the best of each material and avoid any property conflict. This is particularly relevant for the concrete industry as cementitious materials display a very high compressive strength—up to 230 MPa[1]—but a relatively weak flexural strength—approximately 10 times weaker than the compressive strength. This weakness makes standard concrete unsuitable for structural applications required for slabs or bridges; therefore, metallic reinforcing bars are mandatory according to the norms.[2] Over the last decades, numerous studies have been carried out to improve cementitious materials' flexural strength to reduce the systematic use of metallic reinforcing bars. Different strategies have been explored, such as the development of epoxy-modified concrete,[3] the addition of latex suspensions,[4] or crushed tires,[5] but the most promising option is the addition of fibers.[6,7] Fiber-reinforced material is an example of such a hybrid: the fibers are added and mixed with the original cementitious slurry to improve its mechanical properties. This method is not restricted to concrete but is also used in different industries, such as ceramics.[8] Adding a high concentration of fibers in concrete leads to the creation of ultra-high-performance concrete (UHPC), whose flexural strength can reach up to 50 MPa.[9] The main drawbacks of a fiber-reinforced material are: 1) the degradation of the rheological properties of the original paste with the addition of fibers,[10,11] leading to such issues as pumping or casting difficulties; and 2) the price increases of the formulation generated by the addition of fibers.

Fiber-reinforced cementitious composites (FRCC) have been studied regarding rheological and mechanical properties.[12] The fiber's nature impacts the fracture toughness of the composite,[12] mainly depending on the interaction or bond of the fibers with the cementitious matrix. The microcrack formations can be delayed with an increase in the toughness of the composite with polyvinyl alcohol (PVA), refined cellulose (RC),[13] metallics,[14,15] or glass.[16] On the other hand, polypropylene (PP) or polyethylene fibers are not chemically binding to the cementitious matrix. Other natural fibers[17] are now used to reinforce mortar and concrete.

The impact of the fiber aspect ratio, which is defined as the ratio of the length of the fiber to its thickness, on mechanical properties has been studied on PVA fibers,[18] PP,[19,20] and steel.[21] The conclusions differ depending on the type of fiber, demonstrating that for steel fiber at a given concentration, the larger aspect ratio exhibits better performance in terms of either the flexural strength or toughening effect, and for the polymer-type fiber, an optimal form factor has been observed.[22] Several empirical models[23] and machine learning algorithms have been built to predict the impact of the flexural strength on the fiber volume fraction and aspect ratio.[24]

The influence of the fiber volume fraction, rigidity, length, and diameter on the rheological and mechanical properties is described by the fiber factor (*FF*), which can be obtained by multiplying the fiber volume fraction by its aspect ratio.[19]

ACI Materials Journal, V. 121, No. 2, March 2024.

MS No. M-2022-409.R3, doi: 10.14359/51740371, received August 14, 2023, and reviewed under Institute publication policies.

Table 1—Mass concentration per weight and percentage of different components of mortar equivalent concrete

Components	OPC	Limestone	Sand	Water	PCE	Total
Mass, %	22	21.5	44	12	0.5	100
Mass, g	440	430	880	240	12	2000

Table 2—Form factors and maximum packing fraction ϕ_0 of metallic fibers

Fiber types	*L*30	*L*20-2	*L*20-1	*L*15	*L*10	*L*5
Length *L*, mm	30	20	20	15	10	5
Width *w*, mm	1.6	1.6	1	1	1	1
Thickness *d*, μm	29	29	24	24	24	24

Table 3—Equivalent between mass fiber added and solid volume fraction of metallic fibers in standard mortar

Mass fiber, g, added in 2 kg of mortar	15	30	45	60	75	112	150	187	225
Equivalent solid volume fraction, %	0.2	0.4	0.6	0.8	1	1.5	2	2.5	3

The *FF* impact on the rheological properties is the same for all types of fibers, with an increase in the yield stress or decrease in the slump spread as well as an increase in the plastic viscosity.[19,21] The influence of the fiber on the mechanical properties is defined with two critical limits of the *FF*: below a critical factor called *Fc*, the influence of the fiber on the mechanical properties is negligible, and above a density factor called *Fd*, the rheological and mechanical properties are worsened due to the nonuniform dispersal of the fibers. The limits of *Fc* and *Fd* depend on the nature and rigidity of the fibers: 30 and 80, respectively, for glass fibers; 100 and 300 for PP; or 100 and 400 for PVA fibers.[19] There is a further need to understand the mechanism of the flexural strength and viscosity increases with the addition of fibers. This would rationalize the optimization of the concrete formulations. To this goal, the correlations between the composite performances, either mechanical or rheological, are then always made with dimensionless parameters to establish such a correlation based on pure geometrical considerations, linking the rheological and mechanical properties with critical volume fractions, which can be calculated from the fiber form factor.

RESEARCH SIGNIFICANCE

This paper aims to link the mechanical and rheological properties of metallic fiber-reinforced mortar with the organization of the fibers. The characterization of the metallic fibers' concentration is made based on the flexural strength, and the rheological properties of the fresh mixture are made and rescaled on geometrical parameters with a series of six different metallic fibers. The impact of the fiber form factor and concentration on the material's physical properties is studied in a fresh and hardened state, showing that the paste's yield stress evolution and the set mortar's flexural strength are linked with the relative fiber volume fractions.

EXPERIMENTAL INVESTIGATION

Materials and formulations

The rheological and mechanical impacts of the fiber addition are studied on a mortar prepared with a binary binder made of ordinary portland cement (OPC) type CEM I 52.5N and limestone having the same particle-size distribution. Natural siliceous sand with a particle size ranging from 0.1 to 0.5 mm with a specific gravity of 2.6 kg/L and water absorption of 1% was used. Finally, a noncommercial plasticizer of the type of polycarboxylate high-range water-reducing admixture (PCE) with a solid content of 40% and a density of 1.08 kg/L was added at a concentration of 0.5% to obtain a self-leveling mortar. The formulation of the reference mortar is shown in Table 1 in terms of percentage and mass used. A 2 kg mortar mixture was prepared with a water-cement ratio (*w*/*c*) of 0.56 and a water-binder ratio (*w*/*b*) of 0.28. The mixing protocol consists of mixing for 1 minute in a mixer at speed one, then letting the paste rest for 30 seconds, and mixing again at speed two for 2 minutes. The resulting mortar is self-leveling with a density of 2 kg/L.

The fibers used are commercial; they are amorphous metallic fibers for concrete and mortar reinforcement with a density of 7.25 kg/L.[25] A series of six different fibers were tested to study the impact of the form factor on the fibers' rheological and mechanical properties of the mixture. The reference names of the fibers with their equivalent length *L*, width *w*, and thickness *d* are summarized in Table 2.

The different fibers were incorporated in a second step into the self-leveling mortar with a second mixture of 1 minute at speed one. A noncommercial deformer was used to keep the air content below 2% for all the mixtures to avoid the air's negative impact on the mechanical properties. All the fiber concentrations are given in percentage per volume. Table 3 gives the equivalence between mass concentration and volume fraction of the fibers in the mortar mixtures. Due to the high density of the fiber, the mass added for 3% is 223 g for 2 kg of mortar. No sedimentation of the fibers was observed, as confirmed by tomography measurements.

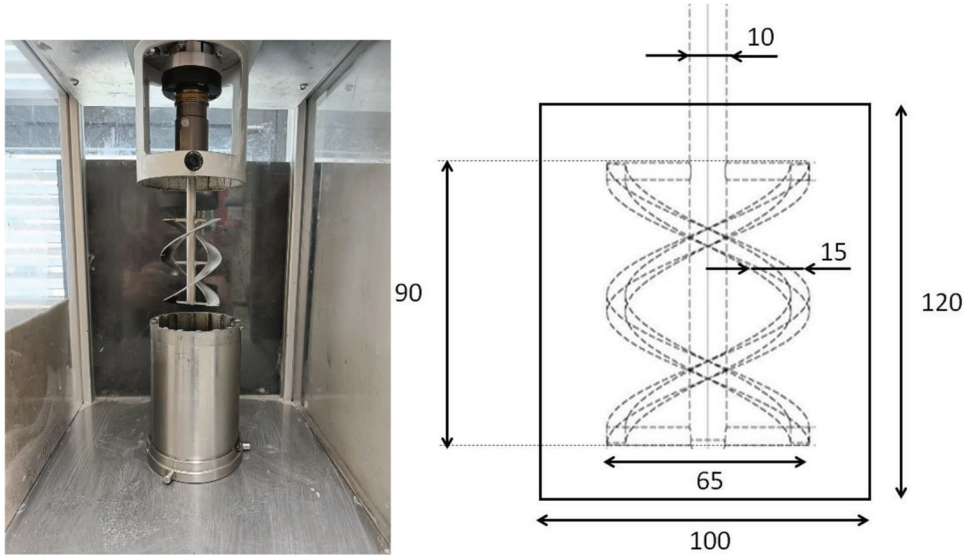

Fig. 1—Concrete rheometer used for measurement of rheological properties of mortar pastes: (left) picture of rheometer with measuring cell; and (right) dimensions of geometry.

Rodlike PVA fiber was used for complementary rheological measurements and validation of theory building on the metal fibers. The ductile monfilament PVA fiber has a diameter of 38 μm, a length of 8 mm, and a density of 1.3 g/cm^3. The PVA fibers are also used to improve the strength properties of concrete and mortar.

Rheological measurements

To compare the rheological and mechanical properties, two different tests have been conducted: 1) rheological with a concrete rheometer; and 2) mechanical, with a three-point flexural test. The rheological properties of the fresh reinforced mortar are measured with a custom-made concrete rheometer represented in the left picture of Fig. 1. It is equipped with a double-helicoidal geometry designed for the rheological measurement of a cement paste, as described in former works,[26-28] and with the dimensions given in the right picture of Fig. 1. The rheometer was calibrated with a calibration oil developed by the National Institute of Standards and Technology (NIST).[29] This calibration allows the quantification of the shear rate and shear stress directly from the measurement of the geometry rotation speed and torque. The measurement protocol is as such: after a pre-shear of 60 seconds at a shear rate $\dot{\gamma}$ of 100 s^{-1} is first applied, the shear stress τ is measured as a function of the shear rate $\dot{\gamma}$, with 30 points evenly distributed in a logarithmic scale from 100 to 0.1 s^{-1}. The measurement is run three times to ensure good reproducibility.

Flexural strength measurements

The mechanical properties of the mortars are measured on prisms of standard dimensions of 4 x 4 x 16 cm. The prisms are stored in a chamber with controlled curing conditions of 68% relative humidity and 23°C for 7 days. After 7 days of curing, the flexural strength σ_f is measured with the three-point bending test method.

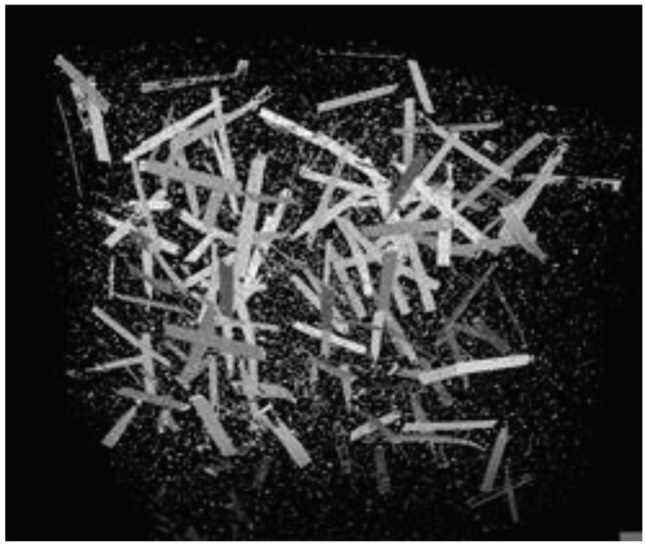

Fig. 2—X-ray tomography of mortar prepared with 1% of L*30. Probe is cube of 40 mm side.*

X-ray tomography

The X-ray tomography imaging was performed with a three-dimensional (3-D) X-ray micro-computed tomography system. The illumination is realized with an X-ray generator with a tungsten filament and a tungsten target, and the detector is a matrix plane sensor consisting of 1920 x 1536 pixels of size 127 x 127 μm. A representation of a 40 mm side sample prepared with 1% of the *L*30 fiber is shown in Fig. 2.

It is very easy to see the metallic fibers. Much smaller objects can also be seen, which are a few microns in size, probably metal oxide particles from the cement, which absorb approximately as much as metal fibers. The metal fibers are not deformed and do not form clusters and appear to be anisotropic without any visible sedimentation, which confirms that the mortar matrix can be reasonably regarded as uniform in nature.

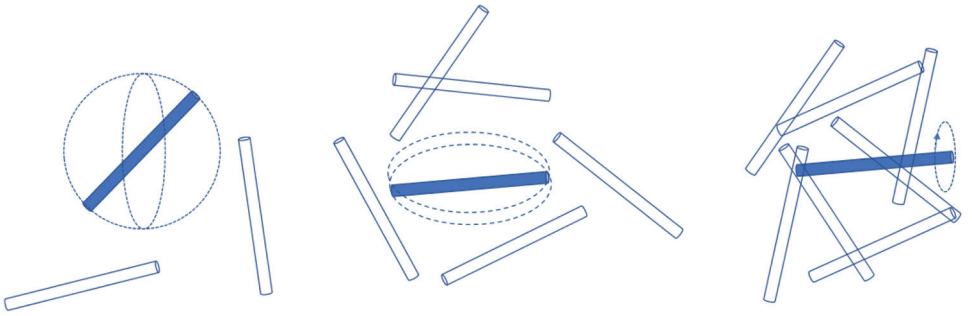

Fig. 3—Three regimes of fibers in solution, from left to right: dilute; semi-dilute, less rotational movement is allowed; and entangled, only rotation on cylindrical axis is possible. (Adapted from Evans and Gibson.[30])

ANALYTICAL INVESTIGATION

The critical flexural strength σ_f is calculated following Eq. (1), with the maximum force applied Fc where the facture of the prism occurs, and with the dimensions of the prism: A = 40 mm and L = 160 mm.

$$\sigma_f = \frac{3FcL}{2A^3} \tag{1}$$

The toughness of the prism, which is the energy the material can absorb by deforming plastically before its rupture, is also calculated using an integral of the force along its displacement δ, as described in Eq. (1).

$$U = \int_0^{\delta_\infty} F(\delta)d\delta \tag{2}$$

All the results shown in the next section are the mean values of the three probes used to measure either the rheological properties or the flexural strength. Error bars correspond to the standard deviation calculated from the experimental data.

To characterize quantitatively the impact of the fiber form factors on the rheological and mechanical properties, the work of Evans and Gibson[30] is adapted, who studied the packing of randomly oriented fibers. This is done by assimilating the metallic fibers to a rodlike fiber with the same length l and an equivalent circular surface with a diameter d_e, calculated by assimilating the rectangular section of the fiber to a circle and defined in Eq. (3).

$$d_e = \sqrt{\frac{4dw}{\pi}} \tag{3}$$

A theoretical packing of the fiber can be calculated if a fiber concentration is considered by unit volume c, which is the number of fibers per unit of volume. Then, according to fiber conservation, the fiber volume fraction ϕ, being the volume occupied by the fibers, is equal to

$$\phi = \frac{\pi d_e^2 lc}{4} \tag{4}$$

Evans and Gibson[30] made a parallel with the liquid-crystal transition, where the particles are constrained by their neighbors. There are three concentration regimes described in Fig. 3: a) the dilute one, where $c \le l^{-3}$ and each fiber can be rotated freely around all axes without touching the others; b) the semi-dilute regime $l^{-3} \le c \le l^{-2}d_e^{-1}$, where a fiber can only rotate in a plane without any contact; and c) the entangled regime $l^{-2}d_e^{-1} \le c \le l^{-1}d_e^{-2}$, where the fibers are only free to rotate around its cylindrical axis of symmetry without touching its neighbors. This corresponds to a nematic ordering.

Table 4—Maximum fiber volume fraction ϕ_0 of different metallic fibers used, as computed from Eq. (5) with k_{th} = 4

Fiber types	*L*30	*L*20-2	*L*20-1	*L*15	*L*10	*L*5
ϕ_0, %	3.3	5.0	3.6	4.8	7.2	14.4

Nevertheless, in this study's system, where the fibers are dispersed in a complex media, they cannot self-organize in a fully nematic state, and their maximum volume fraction will be lower than the maximum volume fraction of the nematic ordering. One needs to consider the maximum volume fraction of randomly oriented fibers, which may be evaluated by considering fibers at low volume fractions and then compressing the system up to the point where it cannot be compressed further without deformation of the fibers. This leads to the result[31] that the maximum number fraction of the rods is

$$\phi_0 = \frac{kd_e}{l} \tag{5}$$

where k is a numerical refactor, which has been numerically evaluated as k_{th} = 4. Experiments show this expression is valid, but experiments disagree on the numerical prefactor when a k_{exp} = 5.3 is measured.[32] It should be noted that both the maximum packing and the transition between disordered and nematic states scale as the inverse of the form factor, FF.

The list of ϕ_0 calculated with the theoretical coefficient k_{th} for all the types of fibers used is given in Table 4.

EXPERIMENTAL RESULTS AND DISCUSSION

Effect of fiber content on flexural strength

The effect of fiber concentration on the flexural strength of the fiber-reinforced mortar was tested, and the evolution of the strength as a function of the applied deformation for different concentrations of the fiber type *L*30 is shown in Fig. 4. One can observe that below a given fiber volume fraction, in the case of the *L*30, ϕ = 0.4%v, the fibers do

not have any significant effect on the mechanical properties, as has already been observed.[33] Above this concentration, the addition of fibers increases the mortar critical flexural strength σ_f, which is doubled with an addition of 1%v of *L*30 fibers, demonstrating the toughening effect of the metallic fibers.

The quantification of the impact of the concentration and form factors of the six different fibers on the critical flexural strength σ_f is analyzed with its representation as a function of the fiber volume fraction, as shown in Fig. 5. The effect of the mechanical performances is highly dependent on the fiber form factors: the shortest fibers (*L*5) have the least effect, and the increase in the critical flexural strength occurs only above concentration 1.5%v, whereas the same increase can be seen at a volume fraction of 0.5%v for the larger fiber (*L*30). It is interesting to notice that while their lengths are different, the duos *L*30 and *L*20-1 and *L*20-2 and *L*15 display very similar behaviors, which means that the relevant parameter is the fiber's form factor and not its length.[34]

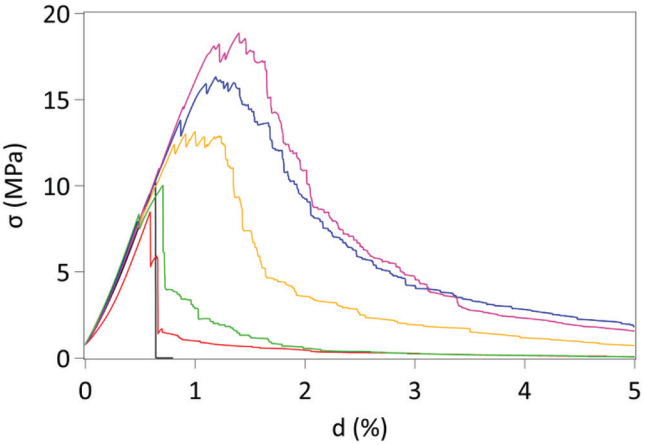

Fig. 4—Strength of reinforced mortar as function of flexural strain for different fiber concentrations at 0, 0.2, 0.4, 0.6, 0.8, and 1% volume fraction from left to right in order of appearance of peak. Tested fiber is L*30, described in Table 2. Maximum strength is taken as critical flexural strength* σ_f *of composite.*

The evolution of the flexural strength confirms that there is a minimum volume fraction required to impact the mechanical properties, which depends on the fiber form factor. The fiber network then affects the mechanical properties as the mechanical effort is transmitted in both the fiber and mortar networks.[35,36]

To identify the mechanisms at play in the increase in the strength of the system, the data of Fig. 5 were rescaled by the maximum packing fraction ϕ_0 displayed in Table 4 to correlate the packing influence of the fibers on the mechanical properties. As ϕ_0 is a function of the ratio d_e/l, each curve is shifted differently according to its form factor, and the evolution of the critical flexural strength as well as the toughness of the samples are represented in Fig. 6 (left). The flexural strength starts to kick off for a ratio of $\phi/\phi_c \approx 0.15$: below this ratio, the fibers do not have any significant effect on the mechanical properties.

Remarkably, all data from the different fibers collapse on a master curve under this rescaling by the maximum packing volume fraction ϕ_0. In particular, the increase in the flexural strength occurs at a similar rescaled volume fraction. This implies that the transition toward the strong reinforcement regime is controlled by the same scaling factor as the maximum packing volume fraction. According to the preceding discussion, it may be identified with the volume fraction transition between the semi-dilute and the entangled regime.

Therefore, according to Eq. (4) and (5), the ratio between ϕ_c and ϕ_0 can be written as

$$\frac{\phi_c}{\phi_0} = \frac{\pi}{4k} \tag{6}$$

The ratio ϕ_c/ϕ_0 is approximately equal to 0.2 and 0.15 with $k_{th} = 4$ and $k_{exp} = 5.3$, respectively. Those values are very close to the experimental values of Fig. 6 and confirm that the fibers start to have a significant impact when their orientational motion in both angular directions is constrained by their neighbors. The same observations are confirmed by the values of the toughness: the effect of the fibers is only controlled by the ratio ϕ_c/ϕ_0, as shown in Fig. 6 (right). The

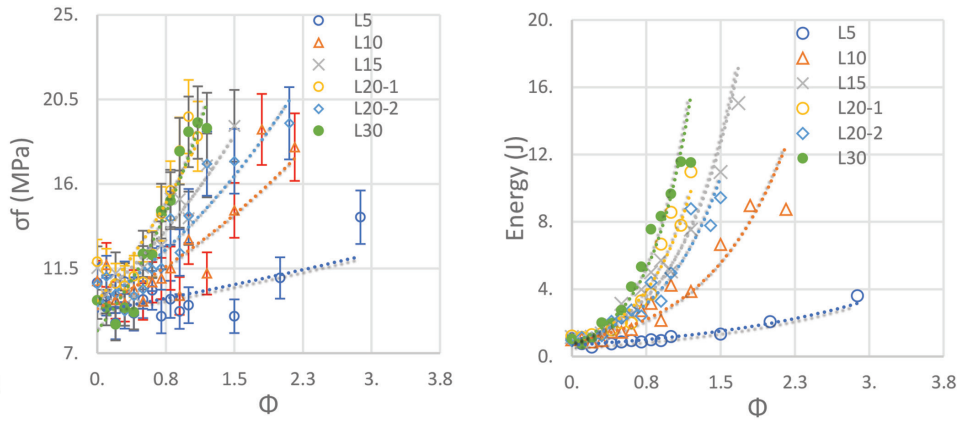

Fig. 5—(Left) Evolution of mean critical flexural strength σ_f *of reinforced mortar has function of solid volume fraction of six different kinds of fibers, described in Table 2; and (right) evolution of total energy, as calculated in Eq. (2) for same fibers. Colors are associated with same fiber, lines are giving trends, and error bars are calculated with average of 10%.*

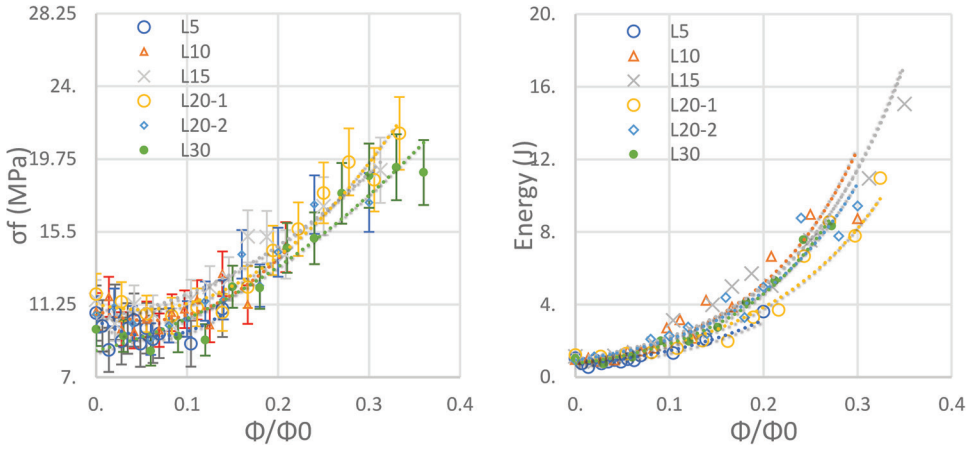

Fig. 6—(Left) Evolution of mean flexural strength of reinforced mortar has function of ratio ϕ/ϕ_0 for six different kinds of fibers, described in Table 2; and (right) evolution of total energy or toughness, as calculated in Eq. (2). Colors are associated with same fiber, lines are giving trends, and error bars are calculated with average of 10% from flexural strength.

toughness curves also collapse in a master curve when the unit ϕ/ϕ_0 is used to rescale the data.

Rheological measurements

As the fiber concentration has been proved to be close to when the hybrid mechanical properties drastically increase, the rheology of the mixture is also supposed to diverge when its volume fraction ϕ tends to some maximum packing fraction that may not be identical to the previously defined ϕ_0, and that this study calls ϕ_m. The increase in the viscosity η with the volume fraction has been widely studied,[37] and the theoretical solution is known for a dilute sphere suspension in a Newtonian fluid of viscosity[38] η_0

$$\eta = \eta_0(1 + 2.5\phi) \tag{7}$$

The problem becomes rapidly difficult to model when the volume fraction increases and becomes close to the maximum packing fraction ϕ_m as the viscosity diverges at the limit.[39] Among all the models, the most commonly used is the Krieger-Dougherty relationship[40]

$$\eta(\phi) = \eta_0(1 - \phi/\phi_m)^{-B\phi_m} \tag{8}$$

with $B = 2.5$ for the hard-sphere Maron-Pierce model,[41] which has the advantage of fixing the power-law exponent and easing the determination of ϕ_m

$$\eta(\phi) = \eta_0(1 - \phi/\phi_m)^{-2} \tag{9}$$

Those models allow the estimation of the maximum packing of a sphere suspension by fitting the experimental data of the evolution of the viscosity with the sphere volume fraction. For the hard sphere, which is the simplest system,[42] $\phi_m \approx 0.64$, but higher experimental values have also been reported.[43] The system becomes even more complex when the suspension is not made out of spheres but rodlike objects: the values of both η_0 and ϕ_m are different from the hard-sphere model.[44,45] Another level of complexity is added to the system as the suspending fluid is non-Newtonian.[39]

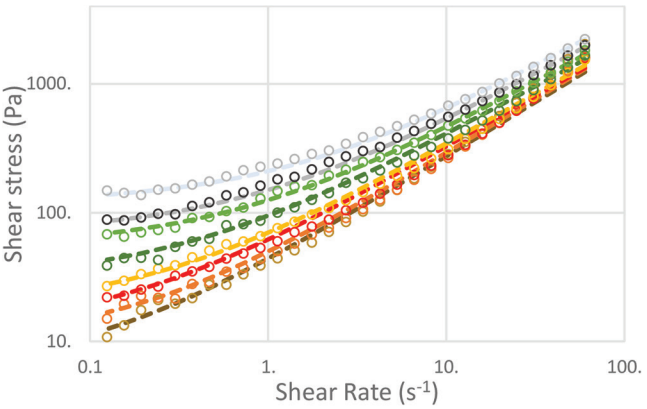

Fig. 7—Evolution of shear stress τ as function of shear rate $\dot{\gamma}$ for fiber-reinforced mortar made with L30 fiber at different fiber concentrations, from bottom to top: ϕ = 0, 0.16, 0.33, 0.5, 0.66, 0.82, 0.99, and 1.15%v. Points are experimental data and dotted lines are Herschel-Bulkley fits.

An example of the evolution of the mortar rheological properties with the amount of *L*30 fibers is represented in Fig. 7. A strong increase in the yield stress τ_y can be observed with the fiber concentrations but also a weaker increase at a high shear rate, which means that the plastic viscosity η_∞ is less dependent on the fiber concentration. It can be explained by a possible fiber alignment with the flow field.[10]

As the mortar is a yield-stress fluid, a Herschel-Bulkley relationship describes the shear stress evolution with the shear rate[46]

$$\tau(\dot{\gamma}) = \tau_y + K\dot{\gamma}^n \tag{10}$$

where K is the consistency index; and n is the flow index. The raw rheological data were fitted with the previous equation to obtain a more precise estimation of the yield stress τ_y, whose mean value was averaged over three experiments. Most of the previously published studies[47-49] focused on the concentration impact on the viscosity and slump flow rather than a direct measure of the yield stress; nevertheless,

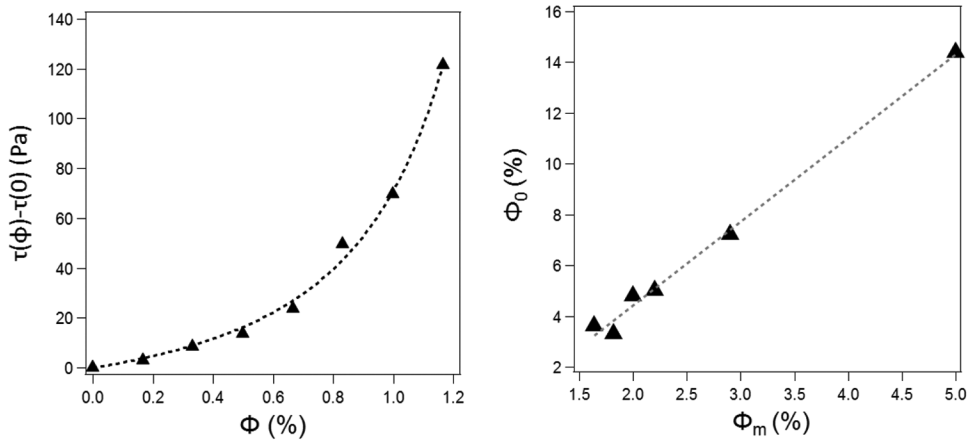

Fig. 8—(Left) Evolution of yield-stress increases $\tau(\phi) - \tau(0)$ as function of L30 fiber concentration ϕ. Data have been fitted using Eq. (11) with $\tau^* = 18.3$ Pa and $\phi_m = 1.2\%$v. (Right) Calculated value ϕ_0 as function of value deduced from rheological measurement ϕ_m for all fibers tested. Dotted line is linear fit of data.

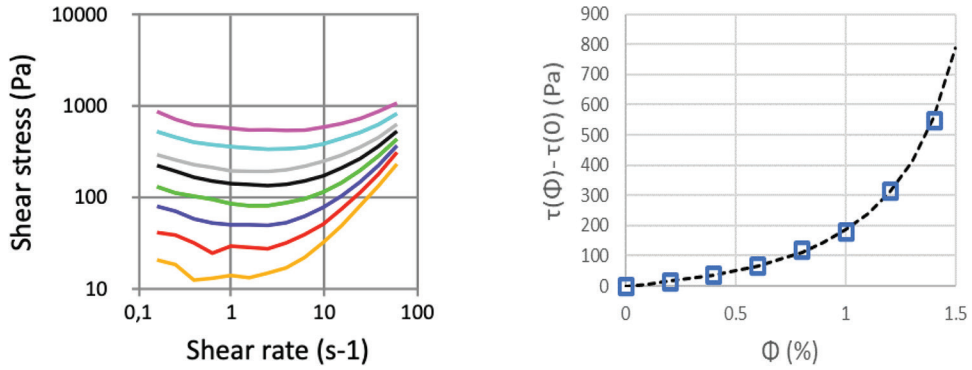

Fig. 9—(Left) Shear stress as function of shear rate for reference mortar made at different concentrations of PVA fibers, from bottom to top: $\phi = 0$, 0.2, 0.4, 0.6, 0.8, 1, 1.2, and 1.4%v; and (right) evolution of yield-stress increases $\tau(\phi) - \tau(0)$ as function of PVA fiber concentration ϕ. Points are extrapolated from experimental data and dotted line from Eq. (11) with τ^* of 70 Pa and ϕ_m of 2.1%.

a derived Maron-Pierce equation has been proposed for its evolution with the particle volume fraction[50]

$$\tau(\phi) = \tau^* \left(\left(1 - \frac{\phi}{\phi_m} \right)^{-2} - 1 \right) \quad (11)$$

This equation has been used to fit the experimental data, and because the previous equation assumed that $\tau(0) = 0$, the fit has been done using $\tau(\phi) = \tau_y(\phi) - \tau_y(0)$, which is represented as a function of the volume fraction on the left side of Fig. 8 for the *L*30 fibers. The points correspond to the experimental data, and the line is the model that perfectly describes the experimental data, demonstrating that the model can be generalized to the complex system. The maximum packing fraction ϕ_m deduced from the fit $\phi_m(L30) = 1.2\%$v appears to be much lower than the maximum packing fraction $\phi_0(L30) = 3.33\%$v obtained from the form factor packing calculation. The same measurements were made for all types of fibers to compare the values of the maximum packing fraction ϕ_m obtained from the rheological measurements and the volume fraction ϕ_0 obtained from the geometrical calculation. The representation of the ϕ_0 as a function of ϕ_m is made in Fig. 8 (right).

Nevertheless, it should be noted that the maximum volume fraction, corresponding to the viscosity divergence ϕ_m, is approximately three times smaller than the theoretical maximum packing fraction of randomly oriented spheres ϕ_0.

To test the generality of the results, experiments were done with other kinds of fibers, in shape and nature, with rodlike PVA fibers. Fibers of diameter 38 μm and length of 8 mm have theoretical maximum packing fractions ϕ_0 of 1.9%v and 2.5%v, calculated with Eq. (5) and with a *k*-factor of 4 and 5.3, respectively. The shear stress evolution as a function of the shear rate in the mortar matrix is represented in Fig. 9 (left), and the measured yield stress is plotted as a function of the volume fraction of the PVA fibers in Fig. 9 (right).

The fitting of the rheological measurements with Eq. (9) (Fig. 9) allows the determination of the experimental critical volume fraction, which is approximately $\phi_m = 2.1\%$v, in between the calculated values of the maximum packing fractions of 1.9%v and 2.5%v. The results obtained with the rodlike fibers are then in the range of the values obtained with Eq. (5), confirming the generality of the results.

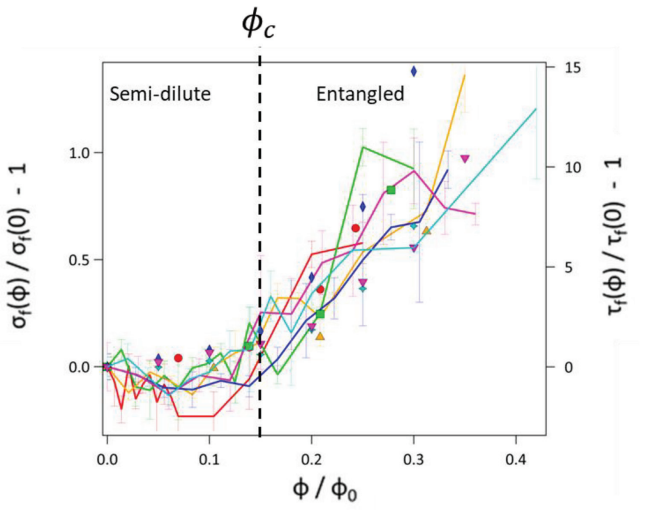

Fig. 10—(Left scale) Evolution of mean normalized flexural strength as function of ϕ/ϕ_0 and maximum packing for six different kinds of fibers, described in Table 2 (line); and (right scale) evolution of mean normalized yield stress as function of ϕ/ϕ_0 (symbol), colors are associated with same fiber. Red: L*5, green:* L*10, orange:* L*15, blue:* L*20-1, green* L*20-2, and pink:* L*30. (Note: Full-color PDF can be accessed at www.concrete.org.)*

Strength-rheology relationship

The data of Fig. 5, 8, and 9 show that both the yield stress τ_y and the critical flexural strength σ_f start to increase drastically around the same volume fraction (ϕ = 0.4%v for the *L*30 fibers). This observation could be a hint that each effect arises from the same phenomenon, which is the outbreak of a fiber network within the mortar sample. To check the similitude between those and make the correlation between the rheological and mechanical properties, the normalized structural strength ($\sigma_f(\phi)/\sigma_f(0) - 1$) and the normalized yield stress ($\tau_f(\phi)/\tau_f(0) - 1$) are represented as a function of the ratio between the volume fraction and the maximum packing ϕ_m calculated from Eq. (5). The results displayed in Fig. 10 show that a similar evolution is observed for both the yield stress and the flexural properties as a function of the ratio between the solid volume fraction and critical volume fraction. A factor of 10 between the scale for the normalized structural strength and the yield stress is observed, meaning that the impact of the relative slope is, therefore, different. This result highlights another remark previously made: the maximum packing fraction deduced from the rheological data using Eq. (11) is always lower than the calculated value from Eq. (5), as can be observed in Fig. 8 (right).

Experimentally, it was nearly impossible to mix and reach fiber volume fractions larger than $0.4\phi/\phi_0$, while it is very easy to prepare hard-sphere suspension up to $0.9\phi/\phi_0$. This could be an argument to advance that the value of the maximum packing deduced from the experimental rheological measurement is closer to the true maximum packing fraction of fibers. Thus, the minimum fiber concentration to trigger their effect can be explained by the theory[30] that has been verified in the experiments: both effects are triggered when $\phi/\phi_0 \approx 0.15$, which corresponds to the transition between the semi-dilute to the entangled regimes represented in Fig. 3. The prediction of the maximum packing fraction of fibers is incorrect because of the modeling of the fibers, which are rectangular cuboids, by rodlike objects, which, as a consequence, could overestimate the real maximum packing fraction. The factor of three for the fiber diameter, obtained between theory and experiment, can be explained with an orientation of the cuboids, leading to an apparent diameter smaller than the one calculated theoretically. The rheological experiments thus allow a quick determination of the fiber form factor, which is needed to determine its impact on the mechanical reinforcement.

CONCLUSIONS

In this paper, the impact of the addition of metallic fibers on both the flexural properties and the rheological properties of a mortar were studied. It was shown experimentally that below a critical concentration, which is only a function of the fiber geometry and defined as the transition between the semi-dilute and entangled regimes, the addition of fibers does not have any significant effect on the improvement of flexural strength. These results were explained by the fact that this critical concentration corresponds to the beginning of an organized network of fibers. Above this critical concentration, both the flexural strength and the yield stress of the fiber-reinforced mortar increase quickly and similarly with the fiber concentration, making the link between flexural properties and rheological properties. No correlation could be made with the plastic viscosity, as the effect of fiber addition is lower at a high shear rate due to their trend to align with the flow but also on the impact of the fibers on the shear thinning of the constitutive paste matrix.

The flexural strength and yield stress increase in parallel as they appear to arise from a common phenomenon based only on the form factor of the fibers. This correlation allows the choosing of the optimal fiber aspect ratio, allowing a quantitative extrapolation and estimation of the flexural properties from the measurement of the yield stress by the calculation of the maximum solid fraction, which is a function of the fiber form factors. The theory was tested with polyvinyl alcohol (PVA) fibers, which have different chemistry and form factors than metal fibers. The maximum packing fractions calculated from the form factor are near the value obtained from the evolution of the yield stress as a function of the fiber volume fraction. Those results could be interesting to ease the formulation of fiber-reinforced mortars as one can calculate the minimum concentration required to improve mechanical properties directly from rheological measurements. This work demonstrates that simple rheological measurements can be performed early to predict and optimize the flexural strength of fiber-reinforced mortar. Further work performed on concrete and highly flexible fiber would allow the generalization of this theory on a more global use of fibers for concrete.

AUTHOR BIOS

Ronan Chometon *received his double engineering degree from ESPCI Paris, Paris, France, in chemical physics, and École Nationale Supérieure des Mines de Paris (MINES Paris – PSL), Paris, France, in materials*

science. He currently works on the development of hybrid interfaces between Li-metal and the electrolyte for solid-state batteries.

Maxime Liard *is a Senior Scientist for Sika Technology AG, Zürich, Switzerland. He received his PhD in physics and chemistry from the Université de Strasbourg, Strasbourg, France, in 2015. His research interests include soft matter, rheology of suspensions, three-dimensional (3-D) printing, and cementitious materials.*

Pascal Hébraud *is a National Centre for Scientific Research (CNRS) Senior Researcher and works at the Institute of Physics and Chemistry of Materials at the Université de Strasbourg. He received his PhD in physics from the Université de Strasbourg in 1998. His research interests include colloids and particle flow and aggregation, which he studies by means of rheology and light scattering techniques.*

Didier Lootens *is a Physico-Chemist and Principal Scientist at Sika Technology. He received his MSc in physico-chemistry from ESPCI Paris, and his PhD in materials science from the Université Pierre et Marie Curie, Paris, France, in 2004. His research interests include early-age characterization of construction materials, rheology, reduction of carbon footprint with supplementary cementitious materials, and formulation optimization.*

ACKNOWLEDGMENTS

The authors thank D. Favier (Institut Charles Sadron [CNRS], Strasbourg, France) for the realization of the X-ray tomography imaging.

NOTATION

A	=	prism width equal to 40 mm
B	=	constant for hard-sphere model of Maron-Pierce,[41] equal to 2.5
c	=	fiber number concentration by unit volume
d	=	thickness of fiber
d_e	=	equivalent diameter of fiber corresponding to circular section
Fc	=	critical factor
F_c	=	maximum flexion force at failure for prism
Fd	=	density factor
FF	=	fiber factor
$F(\delta)$	=	force applied at given displacement
K	=	consistency index
k	=	numerical prefactor[30] for calculation of maximum fiber packing fraction
k_{exp}	=	experimental numerical prefactor k equal to 5.3
k_{th}	=	theoretical numerical prefactor k equal to 4
L	=	prism length equal to 160 mm and section width equal to 40 mm
l	=	equivalent length of fiber
n	=	flow index
U	=	toughness of prism, which is energy material can absorb by deforming plastically before its rupture
w	=	width of fiber
δ	=	displacement or deformation of prism
ϕ	=	fiber volume fraction
ϕ_c	=	fiber volume fraction at dilute/semi-dilute transition
ϕ_m	=	volume fraction corresponding to divergence of viscosity
ϕ_0	=	fiber volume fraction at semi-dilute/tangle transition
	=	shear rate
η	=	viscosity of suspension with or without fiber
η_0	=	Newtonian fluid of viscosity
σ_f	=	critical flexural strength
τ	=	shear stress
τ^*	=	shear stress constant
τ_y	=	yield stress

REFERENCES

1. de Larrard, F., and Sedran, T., "Optimization of Ultra-High-Performance Concrete by the Use of a Packing Model," *Cement and Concrete Research*, V. 24, No. 6, 1994, pp. 997-1009. doi: 10.1016/0008-8846(94)90022-1

2. MacGregor, J. G., *Reinforced Concrete: Mechanics and Design*, third edition, Prentice Hall, Upper Saddle River, NJ, 1997, 939 pp.

3. El-Hawary, M. M., and Abdul-Jaleel, A., "Durability Assessment of Epoxy Modified Concrete," *Construction and Building Materials*, V. 24, No. 8, Aug. 2010, pp. 1523-1528. doi: 10.1016/j.conbuildmat.2010.02.004

4. Shaker, F. A.; El-Dieb, A. S.; and Reda, M. M., "Durability of Styrene-Butadiene Latex Modified Concrete," *Cement and Concrete Research*, V. 27, No. 5, May 1997, pp. 711-720. doi: 10.1016/S0008-8846(97)00055-0

5. Topçu, I. B., "The Properties of Rubberized Concretes," *Cement and Concrete Research*, V. 25, No. 2, Feb. 1995, pp. 304-310. doi: 10.1016/0008-8846(95)00014-3

6. Sivakumar, A., and Santhanam, M., "Mechanical Properties of High Strength Concrete Reinforced with Metallic and Non-Metallic Fibres," *Cement and Concrete Composites*, V. 29, No. 8, Sept. 2007, pp. 603-608. doi: 10.1016/j.cemconcomp.2007.03.006

7. Wafa, F. F., and Ashour, S. A., "Mechanical Properties of High-Strength Fiber Reinforced Concrete," *ACI Materials Journal*, V. 89, No. 5, Sept.-Oct. 1992, pp. 449-455.

8. Bansal, N. P., ed., *Handbook of Ceramic Composites*, Kluwer Academic Publishers, New York, 2005, 554 pp.

9. Acker, P., and Behloul, M., "Ductal® Technology: A Large Spectrum of Properties, A Wide Range of Applications," *Proceedings of the International Symposium on Ultra High Performance Concrete*, M. Schmidt, E. Fehling, and C. Geisenhanslüke, eds., Kassel, Germany, Sept. 2004, pp. 11-23.

10. Petrie, C. J. S., "The Rheology of Fibre Suspensions," *Journal of Non-Newtonian Fluid Mechanics*, V. 87, No. 2-3, Nov. 1999, pp. 369-402. doi: 10.1016/S0377-0257(99)00069-5

11. Maschmeyer, R. O., and Hill, C. T., "Rheology of Concentrated Suspensions of Fibers in Tube Flow. II. An Exploratory Study," *Transactions of The Society of Rheology*, V. 21, No. 2, July 1977, pp. 183-194. doi: 10.1122/1.549453

12. Alrawashdeh, A., and Eren, O., "Mechanical and Physical Characterisation of Steel Fibre Reinforced Self-Compacting Concrete: Different Aspect Ratios and Volume Fractions of Fibres," *Results in Engineering*, V. 13, Mar. 2022, Article No. 100335. doi: 10.1016/j.rineng.2022.100335

13. Nelson, P. K.; Li, V. C.; and Kamada, T., "Fracture Toughness of Microfiber Reinforced Cement Composites," *Journal of Materials in Civil Engineering*, ASCE, V. 14, No. 5, Oct. 2002, pp. 384-391.

14. Ku, D.-O.; Kim, S.-D.; Kim, H.-S.; and Choi, K.-K., "Flexural Performance Characteristics of Amorphous Steel Fiber-Reinforced Concrete," *Journal of the Korea Concrete Institute*, V. 26, No. 4, Aug. 2014, pp. 483-489. doi: 10.4334/JKCI.2014.26.4.483

15. Shin, H.-O.; Kim, K.; Oh, T.; and Yoo, D.-Y., "Effects of Fiber Type and Specimen Thickness on Flexural Behavior of Ultra-High-Performance Fiber-Reinforced Concrete Subjected to Uniaxial and Biaxial Stresses," *Case Studies in Construction Materials*, V. 15, Dec. 2021, Article No. e00726. doi: 10.1016/j.cscm.2021.e00726

16. Pannirselvam, N., and Manivel, S., "Influence of Addition of Glass Fibre on Concrete," *IOP Conference Series: Materials Science and Engineering*, V. 1026, 2021, Article No. 012008. doi: 10.1088/1757-899X/1026/1/012008

17. Araya-Letelier, G.; Antico, F. C.; Carrasco, M.; Rojas, P.; and García-Herrera, C. M., "Effectiveness of New Natural Fibers on Damage-Mechanical Performance of Mortar," *Construction and Building Materials*, V. 152, Oct. 2017, pp. 672-682. doi: 10.1016/j.conbuildmat.2017.07.072

18. Si, W.; Cao, M.; and Li, L., "Establishment of Fiber Factor for Rheological and Mechanical Performance of Polyvinyl Alcohol (PVA) Fiber Reinforced Mortar," *Construction and Building Materials*, V. 265, Dec. 2020, Article No. 120347. doi: 10.1016/j.conbuildmat.2020.120347

19. Pu, B.-C.; Liu, B.; Li, L.; Pang, W.; and Wan, Z., "Influence of Polypropylene Fibre Factor on Flowability and Mechanical Properties of Self-Compacting Geopolymer," *Materials*, V. 14, No. 17, Sept. 2021, Article No. 5025. doi: 10.3390/ma14175025

20. Ibragimov, R.; Bogdanov, R.; Miftakhutdinova, L.; Fediuk, R.; Vatin, N. I.; and de Azevedo, A. R. G., "Effect of Polydisperse Reinforcement on the Fresh and Physical-Mechanical Properties of Self-Compacting Concrete," *Case Studies in Construction Materials*, V. 17, Dec. 2022, Article No. e01188. doi: 10.1016/j.cscm.2022.e01188

21. Hameed, R.; Turatsinze, A.; Duprat, F.; and Sellier, A., "Metallic Fiber Reinforced Concrete: Effect of Fiber Aspect Ratio on the Flexural Properties," *ARPN Journal of Engineering and Applied Sciences*, V. 4, No. 5, July 2009, pp. 67-72.

22. Rao, M. M.; Chowhan, L. N.; and Patro, S. K., "Effect of Aspect Ratio of Fiber in HDPE Reinforced Concrete," *International Journal of Engineering Research & Technology (IJERT)*, V. 8, No. 9, Sept. 2019, pp. 164-171.

23. Teng, L.; Meng, W.; and Khayat, K. H., "Rheology Control of Ultra-High-Performance Concrete Made with Different Fiber Contents," *Cement and Concrete Research*, V. 138, Dec. 2020, Article No. 106222. doi: 10.1016/j.cemconres.2020.106222

24. Kang, M.-C.; Yoo, D.-Y.; and Gupta, R., "Machine Learning-Based Prediction for Compressive and Flexural Strengths of Steel Fiber-Reinforced Concrete," *Construction and Building Materials*, V. 266, Part B, Jan. 2021, Article No. 121117. doi: 10.1016/j.conbuildmat.2020.121117

25. FIBRAFLEX® Documentation, Saint-Gobain, Chalon-sur-Saône, France, www.fibraflex.fr/documents. (last accessed Feb. 16, 2024)

26. Liard, M.; Oblak, L.; Hachim, M.; Vachon, M.; and Lootens, D., "Impact of Viscosity on Hydration Kinetics and Setting Properties of Cementitious Materials," *Advances in Civil Engineering Materials*, V. 3, No. 2, 2014, pp. 117-126. doi: 10.1520/ACEM20130096

27. Toussaint, F.; Roy, C.; and Jézéquel, P.-H., "Reducing Shear Thickening of Cement-Based Suspensions," *Rheologica Acta*, V. 48, No. 8, Oct. 2009, pp. 883-895. doi: 10.1007/s00397-009-0362-z

28. Fabbris, F.; De Carvalho, W.; and Lootens, D., "A Concrete Rheometer: Features and Industrial Applications," *Rheology and Processing of Construction Materials: Proceedings of the 7th RILEM International Conference on Self-Compacting Concrete and 1st RILEM International Conference on Rheology and Processing of Construction Materials*, N. Roussel and H. Bessaies-Bey, eds., Paris, France, 2013, pp. 99-106.

29. Olivas, A.; Ferraris, C. F.; Martys, N. S.; George, W. L.; Garboczi, E. J.; and Toman, B., "Certification of SRM 2493: Standard Reference Mortar for Rheological Measurements," NIST Special Publication 260-187, National Institute of Standards and Technology, Gaithersburg, MD, 2017, 192 pp.

30. Evans, K. E., and Gibson, A. G., "Prediction of the Maximum Packing Fraction Achievable in Randomly Oriented Short-Fibre Composites," *Composites Science and Technology*, V. 25, No. 2, 1986, pp. 149-162. doi: 10.1016/0266-3538(86)90040-0

31. Toll, S., "Packing Mechanics of Fiber Reinforcements," *Polymer Engineering and Science*, V. 38, No. 8, Aug. 1998, pp. 1337-1350. doi: 10.1002/pen.10304

32. Milewski, J. V., "A Study of the Packing of Milled Fibreglass and Glass Beads," *Composites*, V. 4, No. 6, Nov. 1973, pp. 258-265. doi: 10.1016/0010-4361(73)90392-3

33. Lok, T.-S., and Pei, J.-S., "Flexural Behavior of Steel Fiber Reinforced Concrete," *Journal of Materials in Civil Engineering*, ASCE, V. 10, No. 2, May 1998, pp. 86-97. doi: 10.1061/(ASCE)0899-1561(1998)10:2(86)

34. Banthia, N., "A Study of Some Factors Affecting the Fiber–Matrix Bond in Steel Fiber Reinforced Concrete," *Canadian Journal of Civil Engineering*, V. 17, No. 4, Aug. 1990, pp. 610-620. doi: 10.1139/l90-069

35. Johnston, C. D., "Steel Fiber Reinforced Mortar and Concrete: A Review of Mechanical Properties," *Fiber Reinforced Concrete*, SP-44, American Concrete Institute, Farmington Hills, MI, 1974, pp. 127-142.

36. Shannag, M. J.; Brincker, R.; and Hansen, W., "Interfacial (Fiber-Matrix) Properties of High-Strength Mortar (150 MPa) from Fiber Pullout," *ACI Materials Journal*, V. 93, No. 5, Sept.-Oct. 1996, pp. 480-485.

37. Mewis, J., and Wagner, N. J., *Colloidal Suspension Rheology*, Cambridge University Press, Cambridge, UK, 2012.

38. Einstein, A., "Eine neue Bestimmung der Moleküldimensionen," *Annalen der Physik*, V. 324, No. 2, 1906, pp. 289-306. doi: 10.1002/andp.19063240204

39. Mueller, S.; Llewellin, E. W.; and Mader, H. M., "The Rheology of Suspensions of Solid Particles," *Proceedings of the Royal Society A: Mathematical, Physical and Engineering Sciences*, V. 466, No. 2116, Apr. 2010, pp. 1201-1228. doi: 10.1098/rspa.2009.0445

40. Krieger, I. M., and Dougherty, T. J., "A Mechanism for Non-Newtonian Flow in Suspensions of Rigid Spheres," *Transactions of the Society of Rheology*, V. 3, No. 1, 1959, pp. 137-152. doi: 10.1122/1.548848

41. Maron, S. H., and Pierce, P. E., "Application of Ree-Eyring Generalized Flow Theory to Suspensions of Spherical Particles," *Journal of Colloid Science*, V. 11, No. 1, Feb. 1956, pp. 80-95. doi: 10.1016/0095-8522(56)90023-X

42. Rintoul, M. D., and Torquato, S., "Computer Simulations of Dense Hard-Sphere Systems," *The Journal of Chemical Physics*, V. 105, No. 20, Nov. 1996, pp. 9258-9265. doi: 10.1063/1.473004

43. Rutgers, I. R., "Relative Viscosity of Suspensions of Rigid Spheres in Newtonian Liquids," *Rheologica Acta*, V. 2, No. 3, Sept. 1962, pp. 202-210. doi: 10.1007/BF01983952

44. Jeffery, G. B., "The Motion of Ellipsoidal Particles Immersed in a Viscous Fluid," *Proceedings of the Royal Society of London. Series A, Containing Papers of a Mathematical and Physical Character*, V. 102, No. 715, Nov. 1922, pp. 161-179. doi: 10.1098/rspa.1922.0078

45. Brenner, H., "Rheology of a Dilute Suspension of Axisymmetric Brownian Particles," *International Journal of Multiphase Flow*, V. 1, No. 2, Apr. 1974, pp. 195-341. doi: 10.1016/0301-9322(74)90018-4

46. Herschel, W. H., and Bulkley, R., "Konsistenzmessungen von Gummi-Benzollösungen," *Colloid and Polymer Science*, V. 39, No. 4, Aug. 1926, pp. 291-300. doi: 10.1007/BF01432034

47. Gwon, S.; Han, S. H.; Vu, T. D.; Kim, C.; and Shin, M., "Rheological and Mechanical Properties of Kenaf and Jute Fiber-Reinforced Cement Composites," *International Journal of Concrete Structures and Materials*, V. 17, No. 1, Dec. 2023, Article No. 5. doi: 10.1186/s40069-022-00565-1

48. De La Rosa, Á.; Ruiz, G.; Castillo, E.; and Moreno, R., "Probabilistic Assessment of the Dynamic Viscosity of Self-Compacting Steel-Fiber Reinforced Concrete through a Micromechanical Model," *Materials*, V. 15, No. 8, Apr. 2022, Article No. 2763. doi: 10.3390/ma15082763

49. Teng, L.; Huang, H.; Du, J.; and Khayat, K. H., "Prediction of Fiber Orientation and Flexural Performance of UHPC Based on Suspending Mortar Rheology and Casting Method," *Cement and Concrete Composites*, V. 122, Sept. 2021, Article No. 104142. doi: 10.1016/j.cemconcomp.2021.104142

50. Heymann, L.; Peukert, S.; and Aksel, N., "On the Solid-Liquid Transition of Concentrated Suspensions in Transient Shear Flow," *Rheologica Acta*, V. 41, No. 4, Jan. 2002, pp. 307-315. doi: 10.1007/s00397-002-0227-1